Published in final edited form as:
Biomaterials. 2012 July ; 33(21): 5414–5422. doi:10.1016/j.biomaterials.2012.04.032.

Noninvasive monitoring of orthotopic glioblastoma therapy response using RGD-conjugated iron oxide nanoparticles

Fan Zhang[a,1], **Xinglu Huang**[b,1], **Lei Zhu**[b,c], **Ning Guo**[c], **Gang Niu**[b], **Magdalena Swierczewska**[b], **Seulki Lee**[b], **Hong Xu**[d], **Andrew Y. Wang**[d], **Khalid A. Mohamedali**[e], **Michael G. Rosenblum**[e], **Guangming Lu**[a,**], and **Xiaoyuan Chen**[b,c,*]

[a]Department of Radiology, Nanjing Jinling Hospital, Clinical School of Medical College of Nanjing University, Nanjing 210002, China

[b]Laboratory of Molecular Imaging and Nanomedicine (LOMIN), National Institute of Biomedical Imaging and Bioengineering (NIBIB), National Institutes of Health (NIH), Bethesda, MD 20892, USA

[c]Center for Molecular Imaging and Translational Medicine, School of Public Health, Xiamen University, Xiamen 361005, China

[d]Ocean NanoTech, LLC 2143 Worth Lane Springdale, AR 72764, USA

[e]Department of Experimental Therapeutics, The University of Texas M.D. Anderson Cancer Center, Houston, TX 77230, USA

Abstract

Noninvasive imaging techniques have been considered important strategies in the clinic to monitor tumor early response to therapy. In the present study, we applied RGD peptides conjugated to iron oxide nanoparticles (IONP-RGD) as contrast agents in magnetic resonance imaging (MRI) to noninvasively monitor the response of a vascular disrupting agent $VEGF_{121}$/rGel in an orthotopic glioblastoma model. RGD peptides were firstly coupled to IONPs coated with a crosslinked PEGylated amphiphilic triblock copolymer. *In vitro* binding assays confirmed that cellular uptake of particles was mainly dependent on the interaction between RGD and integrin $\alpha_v\beta_3$ of human umbilical vein endothelial cells (HUVEC). The tumor targeting of IONP-RGD was observed in an orthotopic U87 glioblastoma model. Finally, noninvasive monitoring of the tumor response to $VEGF_{121}$/rGel therapy at early stages of treatment was successfully accomplished using IONP-RGD as a contrast agent for MRI, a superior method over common anatomical approaches which are based on tumor size measurements. This preclinical study can accelerate anticancer drug development and promote clinical translation of nanoprobes.

Keywords

Magnetic resonance imaging (MRI); Iron oxide nanoparticles (IONPs); RGD peptides; Tumor targeting; Therapy response

*Corresponding author. Laboratory of Molecular Imaging and Nanomedicine (LOMIN), National Institute of Biomedical Imaging and Bioengineering (NIBIB), National Institutes of Health (NIH), Bethesda, MD 20892, USA. Tel.: +1 301 451 4246. **Corresponding author. cjr.luguangming@vip.163.com (G. Lu), shawn.chen@nih.gov (X. Chen).
[1]These authors contributed equally to this work.

1. Introduction

The detailed information of tumor progression in response to therapy is important to improve patient selection for specific treatment strategies and guides adaptation of treatment at an early stage [1]. Anatomical approaches based on measurements of tumor size are extensively applied for assessing therapy response so far, but significant limitations exist, such as the presence of tumors that cannot be measured, poor measurement reproducibility, and mass lesions that persist following therapy [2]. Noninvasive imaging techniques are emerging more and more as important tools to monitor response to therapies with novel mechanisms of action, often predicting the success of therapy before conventional measurements have changed [3,4]. The development of advanced imaging strategies, although still challenging, not only allow the detection and monitoring of tumor development, but also facilitate a broad understanding of the cellular and molecular events that propagate tumor angiogenesis, as well as those occurring in response to therapy.

A highly versatile device in monitoring tumor progression and therapy response is magnetic resonance imaging (MRI), since this technique provides a high spatial resolution and excellent contrast of opaque soft tissue [5]. However, the low sensitivity of MRI often reduces the success of imaging approaches. Recently, iron oxide nanoparticles (IONPs) have shown their suitability for use as sufficiently high tissue contrast agents for MRI in terms of their intrinsic properties and versatile surface functionality [6–9]. Among these applications, the detection of initial and further development of tumors using IONPs as contrast agents is of particular interest. Glioblastoma (GBM) is the most common form of primary brain tumor, and its aggressive nature and evasiveness to treatments make it one of the most lethal cancers [10,11]. To better develop new theranostic strategies in experimental research, orthotopic GBM models are considered more realistic than common subcutaneous xenografts. However, current strategies are mainly limited by the blood–brain barrier (BBB) of models. Several recent reports have demonstrated the feasibility of IONPs to target orthotopic GBM across the BBB [12,13], but it still remains a challenge to noninvasively assess tumor response to therapeutics using IONPs.

$VEGF_{121}$/rGel is a fusion protein containing $VEGF_{121}$ linked by a flexible G_4S tether to the toxin gelonin (rGel) [14]. Such novel fusion construct has high specificity and cytotoxicity to endothelial cells, and has been successfully used for antiangiogenic therapies in various tumor models [14–16]. In this work, we applied an amphiphilic PEG lipid coated, IONP-RGD conjugate for noninvasive monitoring of tumor progression during $VEGF_{121}$/rGel therapy of orthotopic GBM. The IONPs were firstly functionalized by conjugation with RGD peptides. Subsequently, the specific binding of IONP-RGD to integrin $\alpha_v\beta_3$ was studied *in vitro* and *in vivo*. The damaging effect of $VEGF_{121}$/rGel on angiogenic tumor blood vessels was also confirmed in this study. Finally, monitoring the therapeutic response was explored using IONP-RGD as MRI contrast agents in an orthotopic U87MG model.

2. Materials and methods

2.1. Materials

Iron oxide nanoparticles were obtained from Ocean NanoTech. BS_3 crosslinker was purchased from Thermo Scientific. Arginine-glycine-aspartic acid peptide c(RGDyK) was bought from Anaspec. Disposable PD-10 desalting column was acquired from GE healthcare. The centrifugal filter (30 k cutoff) was bought from Millipore. Mounting medium with DAPI was purchased from Vector Laboratories. Human umbilical vein endothelial cell line (HUVEC) and U87MG human glioblastoma-astrocytoma cell line were purchased from ATCC. Rat anti-mouse CD31, hamster anti-mouse β3 antibody (CD61),

biotinylated anti-rat and anti-hamster IgG secondary antibodies were purchased from BD Bioscience. $VEGF_{121}$/rGel was prepared according to a reported procedure [17].

2.2. Synthesis and characterization of IONP-RGD

Ten nm PEGylated amphiphilic copolymer coated IONPs with amino groups were obtained from Ocean NanoTech. For surface modification of RGD peptide, 2 mg of IONPs was dispersed in 4 ml of borate buffer (pH 9.0). Then, 10 μl of BS_3 crosslinker (10 mg/ml) was added to the solution. After stirring for 30 min at room temperature, the mixture was centrifugated and collected via centrifugal filter (30 k cutoff). The particles were redispersed in PBS buffer solution and collected after centrifuging three times. Subsequently, 0.1 ml of RGD peptide (2 mg/ml) was added in 1 ml of particle solution. The mixture was stirred for 2 h at room temperature. Finally, the particles were purified by PD-10 desalting column and kept in PBS solution. The IONPs were observed by transmission electron microscopy (TEM). The hydrodynamic diameter of IONPs and IONP-RGD were also analyzed by dynamic light scattering (DLS).

2.3. Orthotopic brain tumor model

The procedures for developing an orthotopic brain tumor model were performed according to a protocol approved by the National Institutes of Health Clinical Center Animal Care and Use Committee (NIH CC/ACUC). Briefly, female athymic nude mice (4–6 weeks) were intracranially injected with 1×10^5 U87MG cells in the right frontal lobe at coordinates 1.5 mm lateral from the bregma, 0.5 mm anterior, and 2.5 mm intraparenchymal. Tumor cells were allowed to engraft for the indicated time points, and then *in vivo* MRI were performed to monitor tumor growth.

2.4. Prussian blue staining of IONP-RGD labeled HUVECs

Approximately 1×10^5 HUVECs were seeded in each cell culture chamber for growth overnight. After incubation with 50 μg/ml IONPs or IONP-RGD for the indicated time points, the cells were washed three times with PBS buffer. Subsequently, the cells were stained with Prussian blue solution containing 20% (v/v) hydrochloric acid and 10% (v/v) potassium ferrocyanide solution. After incubation for 40 min at room temperature, the cells were washed twice with PBS buffer and were subjected to incubation with a fast red nuclear staining solution for 10 min. Then, the consecutive dehydrations were performed by 70%, 90% and 100% ethanol, respectively. The slides were washed twice with PBS and then observed with an Olympus microscope.

2.5. In vivo MRI

MRI studies were conducted in a 7 T horizontal bore small animal MRI scanner (Bruker Biospin). All mice were anesthetized with 1–2% isoflurane mixed with pure oxygen via a nose cone and were placed in a stretched supine position with a respiratory sensor. Axial and coronal two-dimensional (2D) fast spin-echo sequence images were first acquired to ensure the imaging position of the implanted tumor. The following parameters were adopted in data acquisition: ① T_1- weighted multislice gradient-echo images: TR/TE = 250/4.5 m s, matrix = 256 × 256, FA = 30°, 9 contiguous slices; ② T_2-weighted multislice spinecho images: TR/TE = 2000/48 m s, matrix = 256 × 256, 9 contiguous slices; ③ T_2*- weighted images: TR/TE =1500/4 m s, matrix = 256 × 256, FA = 30°, 9 contiguous slices; ④ T_2-map: TR = 2000/48 m s, matrix = 256 × 256, 1 slice, T_2 relaxation measurements with TE of 10, 20, 30, 40, 50, 60, 70, 80, 90, 100, 110, 120,130, 140, 150, and 160 ms. For each data set, one slice with comparable locations within the tumor was selected to determine signal intensities. Signal intensities were measured in defined regions of interest (ROIs) with Image J (National Institutes of Health).

For IONP-RGD binding evaluation, the mice with U87MG tumors were injected with IONP-RGD at a dose of 5 mg Fe/kg. Two control experiments were also performed by injection with IONPs and another with IONP-RGD after blocking the target by adding free RGD (IONP-RGD + block) at the same dose. For treatment evaluation, two doses of 12 mg/kg $VEGF_{121}$/rGel were intraperitoneally administered, and then the animals were imaged at 4 days.

Dynamic T_2*-weighted images were performed using the T_2*-weighted method with a temporal resolution of 3.4 s over 70 min. The imaging parameters were: TR/TE = 10/3 m s, flip angle = 45°, FOV = 35 × 35 mm, matrix size = 128 × 128, slice thickness = 1 mm, and NEX = 1. Thirty seconds after the start of the TR-MRI sequence, the particles were administered manually over 30 s. The serial images were normalized by dividing signal intensity (SI) of each image by an average value from4 consecutive pre-injection images collected within the first 40 s of the T_2*-MRI sequence. For quantitative analysis, pre-injection images within the first 40 s were averaged to calculate the initial SI (0). SI (t) represents the intensity yield from post-injection images. The IONP-RGD concentrations ($C_{IONP\text{-}RGD}$) were estimated using the following equation: $C_{INOP\text{-}RGD} = -\ln[SI(t)/SI(0)]/TE$ [18].

2.6. Histological study

2.6.1. Double staining of Prussian blue and CD31/integrin γ_3—Mouse brains were collected in optimal-cutting-temperature (O.C.T.) compound and stored in the freezer at −80 °C. Tissue samples were later cut into 5 μm thick slices. Slides were warmed for 20 min at room temperature after removal from −80 °C freezer and were then fixed with ice-cold acetone for 5 min. After fixation, slides were incubated with 0.3% H_2O_2 solution in PBS for 10 min to block endogenous peroxidase activity. Then slides were rinsed 3 times with PBS (2 min each). Rat anti-mouse CD31 primary antibody diluent (1:50) was subsequently applied to the tissue sections, and the incubation was left at room temperature for 1 h in a humid chamber. After rinsing with PBS (3 × 2 min), a biotinylated anti-rat IgG secondary antibody solution (1:50) was applied, and the mixture was incubated for 30 min at room temperature. The slides were rinsed again with PBS and incubated with streptavidin–HRP solution for 30 min at room temperature. After another washing cycle, the slides were developed with DAB substrate solution until the desired color intensity was reached. Then the resulting slides were subjected to Prussian blue staining. The slides were immersed in staining solution (20% hydrochloric acid and 10% potassium ferrocyanide solution mixture, 1:1 volume ratio) for 20 min, and counterstained with nuclear fast red for 5 min. Afterwards, the slides were dehydrated consecutively with 90%, 95% and 100% EtOH (3 min each), cleared with xylene, and mounted with Permount medium. Double staining with Prussian blue and murine integrin β_3 (CD61) was conducted using the same protocol with the exception of the primary antibodies used. For CD61 staining, hamster anti-mouse CD61 mAb and biotinylated anti-hamster IgG secondary antibody solution were used.

2.6.2. Fluorescence staining and image analysis—Frozen tumor tissue slices (5 μm) were fixed with cold acetone for 20 min and dried in the air for 30 min at room temperature. After blocking with 2% BSA for 30 min, the sections were incubated with primary antibody for 2 h at room temperature and then visualized with dye-conjugated secondary antibodies (1:400). The following primary antibodies against different target antigens were used: rat anti-mouse CD31 antibody (1:300) and hamster anti-mouse CD61 antibody (1:100). After washing 3 × 5 min with PBS, the whole slides were mounted with DAPI-containing mounting medium. Fluorescence images were acquired with an epi-fluorescence microscope (Olympus, X81). Quantitative analysis of positive areas of CD31 and CD 61–positive

vessels was done using Image J. In this context, at least three randomly selected vision fields of each tumor were analyzed.

To visualize and quantify integrin $\alpha_v\beta_3$ expressed by the murine tumor vessels and the tumor stroma, immnohistochemistry was performed following a previous report [19].

2.7. Statistical evaluation

Statistical analysis was performed using the Student's two-tailed *t* test with *p* values ≤ 0.05 considered statistically significant.

3. Results

3.1. Fabrication and characterization of IONPs with RGD peptides

The conjugation of IONPs and c(RGDyK) (RGD) was successfully performed based on the procedures of Fig.1. Briefly, the IONPs were firstly synthesized by modifying the previous methods [19–21]. The amphiphilic copolymer with amino groups was subsequently added to interact with the original oleate coating and form a bilayered structure, rendering the particles water soluble. Such IONPs can be dispersed in various buffer solutions for months without precipitation, indicating good stability. The as-synthesized IONPs were highly-ordered and spherical with a diameter of around 10 nm (Fig. 2A). To evaluate the MRI contrast effect of these particles, a phantom study was also performed with IONPs of elevated concentrations. As shown in Fig. 2B, a clear T_2 signal reduction effect was displayed in a concentration-dependent manner. The linear relation of the concentration of IONPs and T_2 signal was further constructed and demonstrated that a r_2 value of around 187 $m_M^{-1}s^{-1}$, which is much higher than that of Feridex (130 $m_M^{-1}s^{-1}$) under the same condition (data not shown). To conjugate the IONPs with RGD peptides, a crosslinker with NHS esters on both ends was introduced to link the amino groups on the particles with RGD (Fig. 1). The successful conjugation of IONPs and RGD (IONP-RGD) was confirmed by DLS analysis. The average hydrodynamic diameter was increased from 33.4 ± 0.3 nm of the IONPs to 44.7 ± 0.6 nm of the IONPs-RGD (Fig. 2C).

3.2. IONPs and IONP-RGD uptake in HUVEC

To assess the specific binding of particles, the uptake of IONPs, IONP-RGD, and IONP-RGD plus free RGD to block the target (IONPRGD + block) was performed *in vitro* using Prussian blue staining (Fig. 3). After incubation with HUVECs for 10 min, uptake of small amounts of IONP-RGD was observed, whereas there was no significant uptake during IONPs and IONP-RGD + block treatments. The uptake of particles was obviously increased in all three groups after incubation for 1 h, showing the internalization to be time-dependent. However, IONP-RGD + block effectively reduced the amount of blue granules in the cytoplasm of HUVECs.

To further confirm the uptake of particles, an MRI phantom study was also performed after incubation with HUVECs for 10 min and 1 h. Quantitative analysis of the relaxation time of samples showed that the results were consistent with the Prussian blue staining. These results indicate that the accumulation of the particles was specifically mediated by the integrin $\alpha_v\beta_3$ binding.

3.3. Evaluation of integrin $\alpha_v\beta_3$ binding in an orthotopic glioblastoma model

To better understand the capability of the particles to bind integrin $\alpha_v\beta_3$ *in vivo*, an orthotopic glioblastoma model was firstly established by inoculating 1×10^5 U87MG cells in the right frontal lobe. The tumor model was confirmed by H&E histological examination after tumor inoculation for 3–4 weeks (Supporting information Fig. S1). The mice were

subsequently subjected to MRI studies on a 7.0 T small animal MRI system. IONP-RGD, IONPs and IONP-RGD + block were intravenously administrated at a dose of 5 mg Fe/kg, and T_2*-weighted fast spin-echo images pre- and 6 h post-injection were acquired. As displayed in Fig. 4A, a dramatic signal drop was observed at the tumor area (indicated by white circles) after the injection of IONP-RGD, while only a marginal signal drop was witnessed in mice injected with IONPs. Moreover, there was no obvious signal drop observed in the IONPRGD + block group. Quantitative analysis of T_2 relaxation time also indicated that the post-injection signal was definitely decreased compared to the pre-injection signal of the IONP-RGD group ($p < 0.01$), whereas the signal of both IONPs and IONP-RGD + block group exhibited no obvious changes. The results demonstrate that the binding capacity of IONPs was dependent on the interaction between RGD peptides and integrin $\alpha_v\beta_3$.

To further confirm the targeting specificity, the mice were sacrificed 6 h post-injection. After preparing frozen tissue slices, CD31/CD61 (integrin $\alpha_v\beta_3$) and Prussian blue double staining was performed. The perfect overlap of IONPs (blue) and CD61 (brown) positive staining was observed in tumor blood vessels of the IONPRGD group, while little superimposition of IONPs and CD61 were found in the IONPs and IONP-RGD + block groups (Fig. 5). Additionally, Prussian blue and CD31 double staining confirmed the particles were mainly attached to the interior of the blood vessel surface. These results indicate that the particle homing is indeed specifically mediated by RGD–blood vessel integrin interaction.

3.4. Effect of $VEGF_{121}$/rGel on the integrin $\alpha_v\beta_3$ expression of tumor angiogenic blood vessels

To study the effect of $VEGF_{121}$/rGel on orthotopic U87MG tumor growth, two doses of $VEGF_{121}$/rGel were firstly administered intraperitoneally (i.p.) at day 0 and day 2 after tumor inoculation. Then, the animals were imaged post-treatment for 4 days. Fig. 6A shows a time-dependent increase of tumor volume in both $VEGF_{121}$/rGel treated and untreated groups. However, U87MG tumor was inhibited by $VEGF_{121}$/rGel compared with the control group. A significant difference in tumor volume was observed at 7 days between the treatment group and the control group ($p < 0.01$).Furthermore, there was no significant body weight loss observed during the treatment process, indicating that $VEGF_{121}$/rGel had no observable side effects at the dosage used during this study.

To validate the inhibition effect of $VEGF_{121}$/rGel histologically, the presence of tumor angiogenic blood vessels and integrin $\alpha_v\beta_3$ expression were investigated. As demonstrated by immunohistochemistry (Fig. 6B), the untreated group exhibited significantly higher CD31-positive area fractions, which are highly related to tumor angiogenic blood vessels, than in the $VEGF_{121}$/rGel treated group. The anti-mouse-CD61 antibody was also used to visualize and quantify murine integrin $\alpha_v\beta_3$ expression by immunofluorescence in frozen tissue slices (Fig. 6C). Intact tumor blood vessels were observed in the untreated group, whereas an interrupted distribution was shown in the treated group. It was also observed that the integrin expression was co-localized with the distribution of tumor blood vessels. For the untreated group, the positive area of both CD31 and CD61 expression was significantly higher than the treated group ($p < 0.05$) (Fig. 6D). These results confirm the $VEGF_{121}$/rGel damaged tumor angiogenic blood vessels and inhibited integrin expression.

3.5. Dynamic monitoring of orthotopic glioblastoma therapy response by MRI

To noninvasively monitor the therapy response of orthotopic GBM, $VEGF_{121}$/rGel was used to treat GBM by destroying tumor angiogenic blood vessels. After treatment for 4 days, T_2*-weighted images of pre- and 6 h post-injection were acquired in both untreated and

$VEGF_{121}$/rGel groups. As shown in Fig. 7A, compared with pre-injection signals of IONP-RGD, the post-injection signal in tumor areas was obviously decreased in the treated group. However, there was no significant signal change in the untreated group. Quantitative analysis found that the relaxation time ($1/T_2$) of the untreated group was 1.3 ± 0.27 fold of the treated group ($p < 0.01$) (Fig. 7B).

To further understand the monitoring information by MRI, a dynamic signal reduction was investigated in the untreated and treated groups. Dynamic T_2*-weighted data was collected at various time points from 0 to 70 min. The representative images over time are displayed in Fig. 8A. A fast and obvious accumulation of IONPRGD was observed in tumor areas of the untreated group, showing a clear profile of GBM with time-dependent signal intensity. Maximum T_2 signal of the untreated group was observed at 2 min after injection of IONP-RGD, which subsequently decreased over time (Fig. 8B). Compared to baseline, only a small signal decrease in the treated group was detected. These results demonstrate that IONP-RGD can be used for noninvasive monitoring of therapeutic response by orthotopic GBM using MRI.

4. Discussion

In the present study, an amphiphilic copolymer was utilized to coat oleate-coated IONPs and render the particles water soluble and functionalizable. Our previous report demonstrates that such phase transfer and surface modification are straightforward, with high throughput and high yield [19]. In view of amino groups coating the IONPs surface, BS_3 crosslinker was introduced to conjugate the amino groups of the RGD peptide to the IONPs. To reduce the chance of crosslinking among nanoparticles, the concentration of IONPs was kept at 0.5 mg/ml during the conjugation procedure. With such a controllable conjugation, we found the diameter of about 90% of IONPs was less than 50 nm (Fig. 2C), which is suitable for *in vivo* tumor targeting.

Cell adhesion molecules such as integrin $\alpha_v\beta_3$ are overexpressed in activated and proliferating endothelial cells [22]. Various tumor cells, such as gliomas [23,24], ovarian carcinomas [25], and breast carcinomas [26], also highly express integrin $\alpha_v\beta_3$. Therefore, the ability to noninvasively detect integrin $\alpha_v\beta_3$ expression in living subjects would allow a better characterization of tumors and help to identify tumor regions with higher aggressiveness. RGD peptides are one of the most popular ligands that target integrin $\alpha_v\beta_3$ [27]. Therefore, RGD conjugates can be designed for specific tumor targeting without the need of extravasation and diffusion in the tumor interstitial space. When conjugated to radiotracers [28], fluorescent markers [29,30], or magnetic NPs [23,31], RGD has been used for the detection of tumor angiogenesis and tumor metastasis.We and others have shown the specific targeting of angiogenic blood vessels [32,33] or tumor cells [19] with IONP-RGD, which was specifically dependent on RGD peptides binding to integrin $\alpha_v\beta_3$ (Fig. 4). Most importantly, IONP-RGD can specifically target orthotopic GBM across the blood brain barrier [12]. The BBB represents one of the most exclusive biological barriers encountered in the treatment of neurologic diseases, limiting the delivery of a vast majority of potential diagnostic agents and therapeutics. Recent studies have indicated that BBB passage by NPs was dictated by hydrodynamic size. For example, a recent study indicated that dendrimer nanoparticles with sizes less than 12 nm were able to permeate the tumor BBB, while larger ones could not [34]. However, Veiseh et al. demonstrated that IONPs with diameters of 33 nm have the ability to cross the BBB and specifically target brain tumors [12]. Herein, we showed the excellent tumor targeting effect of IONP-RGD with a hydrodynamic diameter of 45 nm (Fig. 2). Therefore, the permeability of NPs to BBB is dependent not only on the hydrodynamic diameter, but also on other properties of the NP. The specific mechanisms for

BBB penetration by NPs have yet to be elucidated. One possible explanation is that the integrity of the BBB may be damaged in orthotopic GBM.

$VEGF_{121}$/rGel fusion protein is a vascular disruptive agent composed of the VEGF-A isoform VEGF121 and a recombinant plant toxin gelonin (rGel) [14]. This novel vasculature-targeting fusion protein has been shown to inhibit various tumor growth with low systemic toxicity, including melanoma, GBM, prostate, breast, and bladder tumor models [15]. Our previous study assessed the antitumor effects of $VEGF_{121}$/rGel in an orthotopic GBM mouse model by use of noninvasive *in vivo* bioluminescence imaging, MRI, and PET [16]. In this current study, the growth of orthotopic GBM was also inhibited by $VEGF_{121}$/rGel (Fig. 6A). It was shown the $VEGF_{121}$/ rGel disrupted tumor angiogenic blood vessels and inhibited integrin $\alpha_v\beta_3$ expression (Fig. 6B–D). However, many new antiangiogenic drugs are principally cytostatic and do not necessarily cause large reductions in tumor volume in a short time scale, even if they are effective, which reduces the usefulness of anatomic measures in monitoring response to such agents. To better monitor treatment efficacy, a critical challenge in future clinical application of $VEGF_{121}$/rGel and other antiangiogenic therapies is to develop effective noninvasive *in vivo* imaging techniques. Recently, we applied PET probes to noninvasively monitor glucose metabolism, cellular proliferation, tumor hypoxia and angiogenesis during $VEGF_{121}$/rGel therapy of breast cancer [35]. However, it is still a challenge to monitor therapeutic outcomes of orthotopic brain tumors. This study explored the feasibility of monitoring the therapeutic response of $VEGF_{121}$/rGel therapy in an orthotopic GBM model using IONPs as MRI contrast agents. To better demonstrate the advantages of noninvasive monitoring of antiangiogenic therapy response over common anatomical approaches that are based on measurements of tumor size, a time point of 4 days post-treatment was chosen to study the therapeutic outcome of $VEGF_{121}$/rGel therapy by MRI. As shown in Fig. 7, the definite therapeutic outcome of $VEGF_{121}$/rGel therapy is observed, even though the tumor volume was not significantly changed compared with the control ($p > 0.05$). Such results indicate the potential advantages of IONPs to noninvasively monitor the early response of tumors to therapy in the clinic. The monitoring ability of the therapeutic response was further confirmed by dynamic MRI (Fig. 8). Fig. 8A showed a significant difference of $1/T_2$ signal between the untreated and $VEGF_{121}$/rGel therapy treated group. The difference in the $1/T_2$ signal occurs because the signal is dependent on the density of tumor blood vessels. In other words, the results also demonstrate an excellent antiangiogenic therapy of $VEGF_{121}$/rGel. Furthermore, the $1/T_2$ signal of the tumor area in the untreated group was immediately increased post-injection of IONP-RGD, and then decreased until reaching equilibrium over time. An explanation for this phenomenon is that the signal was mainly derived from the high concentration of IONP-RGD in blood at early time points post-injection, and not due to the particles binding to integrin $\alpha_v\beta_3$ of the blood vessels. With the clearance of particles, only IONP-RGD binding to blood vessels remained in tumor areas and the signal did not change over time.

5. Conclusion

We have successfully accomplished *in vivo* noninvasive monitoring of therapeutic response to $VEGF_{121}$/rGel therapy using IONPs as MRI contrast agents in an orthotopic GBM model. The results show that IONP-RGD not only target GBM by binding to integrin $\alpha_v\beta_3$ of angiogenic blood vessels, but also cross BBB to penetrate the tumor. Most importantly, we also demonstrated the feasibility of using IONP-RGD for noninvasive monitoring of early tumor responses to antiangiogenic therapies, showing higher sensitivity than common approaches based on measurements of tumor size. Undoubtedly, such results are important in clinical oncology to reduce side effects and save costs during treatment, especially with

the growing number of alternative treatment regimens that are only effective in select subgroups of patients.

Supplementary Material

Refer to Web version on PubMed Central for supplementary material.

Acknowledgments

This work was supported in part, by the Intramural Research Program of the NIBIB, NIH, NCI R41CA137960-01, the Henry M. Jackson Foundation, the International Cooperative Program of the National Science Foundation of China (NSFC) (81028009), and the NSFC grant No. 30930028.

Appendix A. Supplementary material

Supplementary data related to this article can be found online at doi:10.1016/j.biomaterials.2012.04.032.

References

1. Weber WA. Assessing tumor response to therapy. J Nucl Med. 2009; 1(50 Suppl):1S–10S. [PubMed: 19380403]
2. Husband JE, Schwartz LH, Spencer J, Ollivier L, King DM, Johnson R, et al. Evaluation of the response to treatment of solid tumours - a consensus statement of the International Cancer Imaging Society. Br J Cancer. 2004; 90(12):2256–2260. [PubMed: 15150551]
3. Han Z, Fu A, Wang H, Diaz R, Geng L, Onishko H, et al. Noninvasive assessment of cancer response to therapy. Nat Med. 2008; 14(3):343–349. [PubMed: 18297085]
4. Day SE, Kettunen MI, Gallagher FA, Hu DE, Lerche M, Wolber J, et al. Detecting tumor response to treatment using hyperpolarized 13C magnetic resonance imaging and spectroscopy. Nat Med. 2007; 13(11):1382–1387. [PubMed: 17965722]
5. de Langen AJ, van den Boogaart V, Lubberink M, Backes WH, Marcus JT, van Tinteren H, et al. Monitoring response to antiangiogenic therapy in non-small cell lung cancer using imaging markers derived from PET and dynamic contrast-enhanced MRI. J Nucl Med. 2011; 52(1):48–55. [PubMed: 21149474]
6. Lee N, Hyeon T. Designed synthesis of uniformly sized iron oxide nano-particles for efficient magnetic resonance imaging contrast agents. Chem Soc Rev. 2012; 41(7):2575–2589. [PubMed: 22138852]
7. Huang J, Zhong X, Wang L, Yang L, Mao H. Improving the magnetic resonance imaging contrast and detection methods with engineered magnetic nano-particles. Theranostics. 2012; 2(1):86–102. [PubMed: 22272222]
8. Zhen Z, Xie J. Development of manganese-based nanoparticles as contrast probes for magnetic resonance imaging. Theranostics. 2012; 2(1):45–54. [PubMed: 22272218]
9. Huang X, Zhuang J, Chen D, Liu H, Tang F, Yan X, et al. General strategy for designing functionalized magnetic microspheres for different bioapplications. Langmuir. 2009; 25(19):11657–11663. [PubMed: 19694417]
10. Gajbhiye V, Jain NK. The treatment of Glioblastoma Xenografts by surfactant conjugated dendritic nanoconjugates. Biomaterials. 2011; 32(26):6213–6225. [PubMed: 21616528]
11. Tzeng SY, Guerrero-Cazares H, Martinez EE, Sunshine JC, Quinones-Hinojosa A, Green JJ. Non-viral gene delivery nanoparticles based on poly(β-amino esters) for treatment of glioblastoma. Biomaterials. 2011; 32(23):5402–5410. [PubMed: 21536325]
12. Veiseh O, Sun C, Fang C, Bhattarai N, Gunn J, Kievit F, et al. Specific targeting of brain tumors with an optical/magnetic resonance imaging nanoprobe across the blood-brain barrier. Cancer Res. 2009; 69(15):6200–6207. [PubMed: 19638572]

13. Dilnawaz F, Singh A, Mewar S, Sharma U, Jagannathan NR, Sahoo SK. The transport of non-surfactant based paclitaxel loaded magnetic nanoparticles across the blood brain barrier in a rat model. Biomaterials. 2012; 33(10):2936–2951. [PubMed: 22264522]
14. Veenendaal LM, Jin H, Ran S, Cheung L, Navone N, Marks JW, et al. In vitro and in vivo studies of a $VEGF_{121}$/rGelonin chimeric fusion toxin targeting the neovasculature of solid tumors. Proc Natl Acad Sci U S A. 2002; 99(12):7866–7871. [PubMed: 12060733]
15. Ran S, Mohamedali KA, Luster TA, Thorpe PE, Rosenblum MG. The vascular-ablative agent $VEGF_{121}$/rGel inhibits pulmonary metastases of MDA-MB-231 breast tumors. Neoplasia. 2005; 7(5):486–496. [PubMed: 15967101]
16. Hsu AR, Cai W, Veeravagu A, Mohamedali KA, Chen K, Kim S, et al. Multi-modality molecular imaging of glioblastoma growth inhibition with vasculature-targeting fusion toxin $VEGF_{121}$/rGel. J Nucl Med. 2007; 48(3):445–454. [PubMed: 17332623]
17. Kim S, Mohamedali KA, Cheung LH, Rosenblum MG. Overexpression of biologically active $VEGF_{121}$ fusion proteins in Escherichia coli. J Biotechnol. 2007; 128(3):638–647. [PubMed: 17218033]
18. Rosen BR, Belliveau JW, Vevea JM, Brady TJ. Perfusion imaging with NMR contrast agents. Magn Reson Med. 1990; 14(2):249–265. [PubMed: 2345506]
19. Chen K, Xie J, Xu H, Behera D, Michalski MH, Biswal S, et al. Triblock copolymer coated iron oxide nanoparticle conjugate for tumor integrin targeting. Biomaterials. 2009; 30(36):6912–6919. [PubMed: 19773081]
20. Park J, An K, Hwang Y, Park JG, Noh HJ, Kim JY, et al. Ultra-large-scale syntheses of monodisperse nanocrystals. Nat Mater. 2004; 3(12):891–895. [PubMed: 15568032]
21. Yu WW, Falkner JC, Yavuz CT, Colvin VL. Synthesis of monodisperse iron oxide nanocrystals by thermal decomposition of iron carboxylate salts. Chem Commun (Camb). 2004; (20):2306–2307. [PubMed: 15489993]
22. Weis SM, Cheresh DA. Tumor angiogenesis: molecular pathways and therapeutic targets. Nat Med. 2011; 17(11):1359–1370. [PubMed: 22064426]
23. Kiessling F, Huppert J, Zhang C, Jayapaul J, Zwick S, Woenne EC, et al. RGD-labeled USPIO inhibits adhesion and endocytotic activity of αvβ3-integrin-expressing glioma cells and only accumulates in the vascular tumor compartment. Radiology. 2009; 253(2):462–469. [PubMed: 19789239]
24. Schnell O, Krebs B, Carlsen J, Miederer I, Goetz C, Goldbrunner RH, et al. Imaging of integrin αvβ3 expression in patients with malignant glioma by [18F] Galacto-RGD positron emission tomography. Neuro Oncol. 2009; 11(6):861–870. [PubMed: 19401596]
25. Cruet-Hennequart S, Maubant S, Luis J, Gauduchon P, Staedel C, Dedhar S. αv integrins regulate cell proliferation through integrin-linked kinase (ILK) in ovarian cancer cells. Oncogene. 2003; 22(11):1688–1702. [PubMed: 12642872]
26. Yang C, Hayashida T, Forster N, Li C, Shen D, Maheswaran S, et al. The integrin αvβ3/5 ligand MFG-E8 is a p63/p73 target gene in triple-negative breast cancers but exhibits suppressive functions in ER(+) and erbB2(+) breast cancers. Cancer Res. 2011; 71(3):937–945. [PubMed: 21127199]
27. Ye Y, Chen X. Integrin targeting for tumor optical imaging. Theranostics. 2011; 1:102–126. [PubMed: 21546996]
28. Zhou Y, Chakraborty S, Liu S. Radiolabeled Cyclic RGD peptides as radiotracers for imaging tumors and Thrombosis by SPECT. Theranostics. 2011; 1:58–82. [PubMed: 21547153]
29. Hsu AR, Hou LC, Veeravagu A, Greve JM, Vogel H, Tse V, et al. In vivo near-infrared fluorescence imaging of integrin αvβ3 in an orthotopic glioblastoma model. Mol Imaging Biol. 2006; 8(6):315–323. [PubMed: 17053862]
30. Chen X, Conti PS, Moats RA. In vivo near-infrared fluorescence imaging of integrin αvβ3 in brain tumor xenografts. Cancer Res. 2004; 64(21):8009–8014. [PubMed: 15520209]
31. Gianella A, Jarzyna PA, Mani V, Ramachandran S, Calcagno C, Tang J, et al. Multifunctional nanoemulsion platform for imaging guided therapy evaluated in experimental cancer. ACS Nano. 2011; 5(6):4422–4433. [PubMed: 21557611]

32. Zhang C, Jugold M, Woenne EC, Lammers T, Morgenstern B, Mueller MM, et al. Specific targeting of tumor angiogenesis by RGD-conjugated ultrasmall superparamagnetic iron oxide particles using a clinical 1.5-T magnetic resonance scanner. Cancer Res. 2007; 67(4):1555–1562. [PubMed: 17308094]

33. Li J, Zhang C, Yang K, Liu P, Xu LX. SPIO-RGD nanoparticles as a molecular targeting probe for imaging tumor angiogenesis using synchrotron radiation. J Synchrotron Radiat. 2011; 18(Pt 4): 612–616. [PubMed: 21685679]

34. Sarin H, Kanevsky AS, Wu H, Brimacombe KR, Fung SH, Sousa AA, et al. Effective transvascular delivery of nanoparticles across the blood-brain tumor barrier into malignant glioma cells. J Transl Med. 2008; 6:80. [PubMed: 19094226]

35. Yang M, Gao H, Sun X, Yan Y, Quan Q, Zhang W, et al. Multiplexed PET probes for imaging breast cancer early response to VEGF/rGel treatment. Mol Pharm. 2011; 8(2):621–628. [PubMed: 21280671]

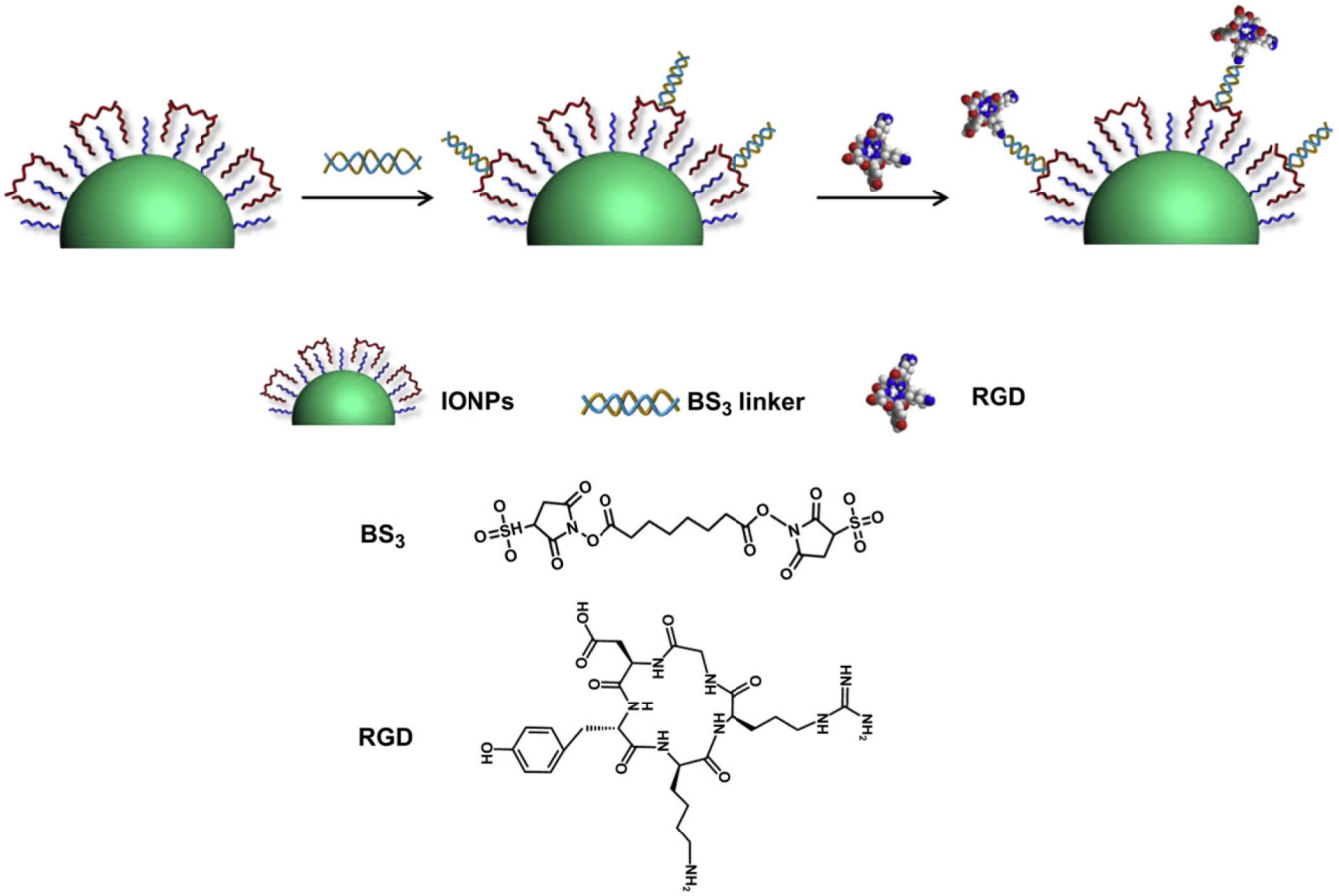

Fig. 1.
Schematic illustration of the conjugation of IONPs with RGD peptides.

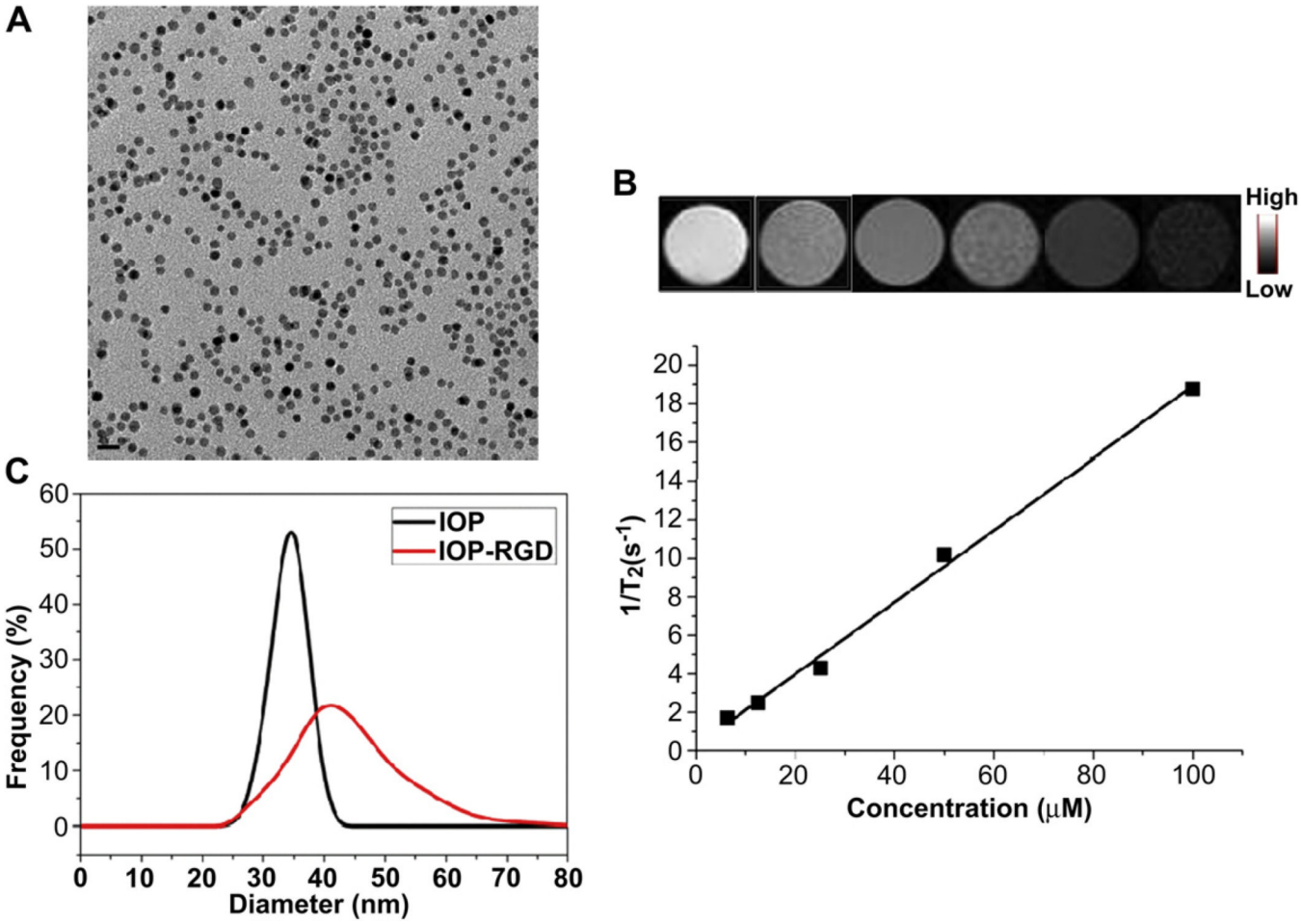

Fig. 2.

Characterization of IONPs and IONP-RGD (A) TEM of IONPs (B) T_2^*-weighted phantom images of IONPs at different Fe concentration. Top, T_2^*-weighted phantom images; Bottom, $1/T_2$ vs. Fe concentration curve of IONPs.

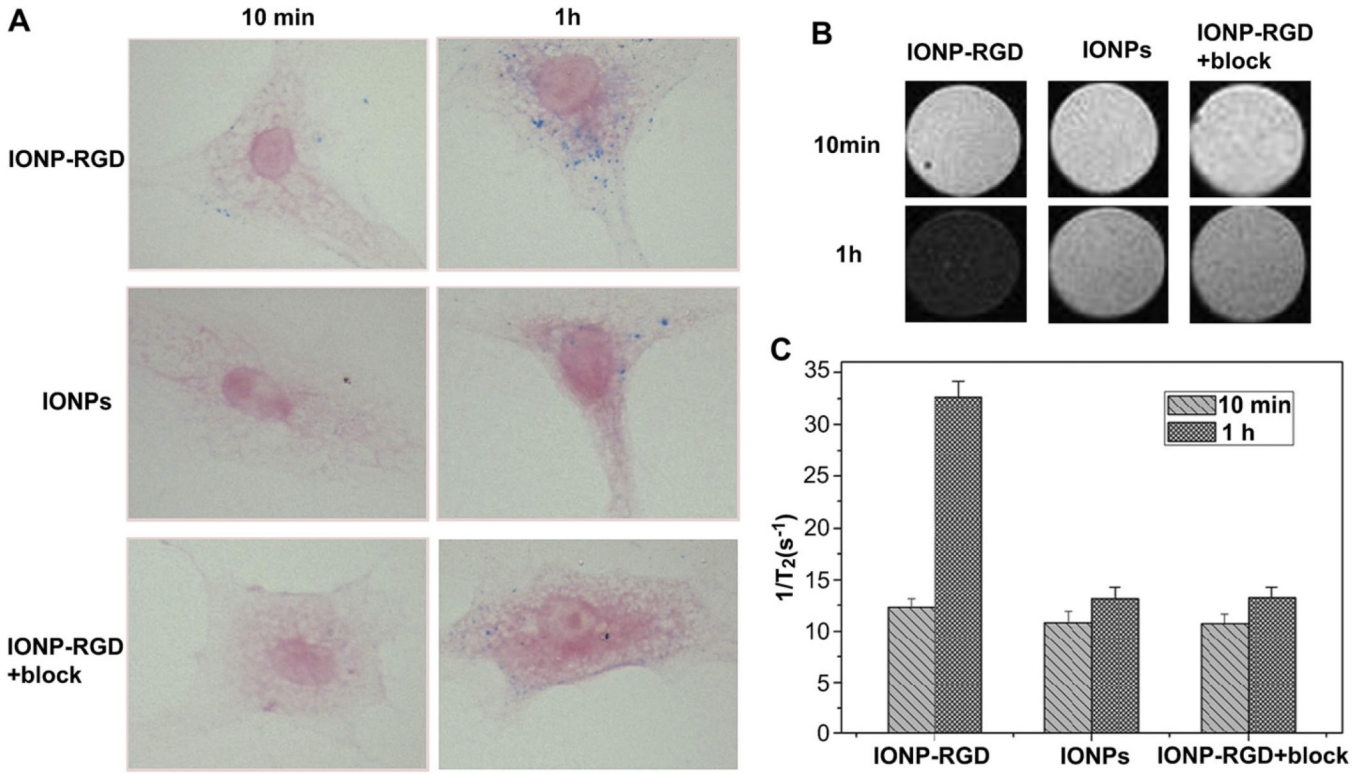

Fig. 3.

Cellular uptake of particles in HUVECs. The IONPs, IONP-RGD and IONP-RGD + block were incubated with HUVECs for 10 min and 1 h, respectively. Cellular uptake was evaluated by (A) Prussian blue staining and (B) T_2-weighted phantom images (C) Quantitative analysis of relaxation time of T_2^*-weighted phantom images.

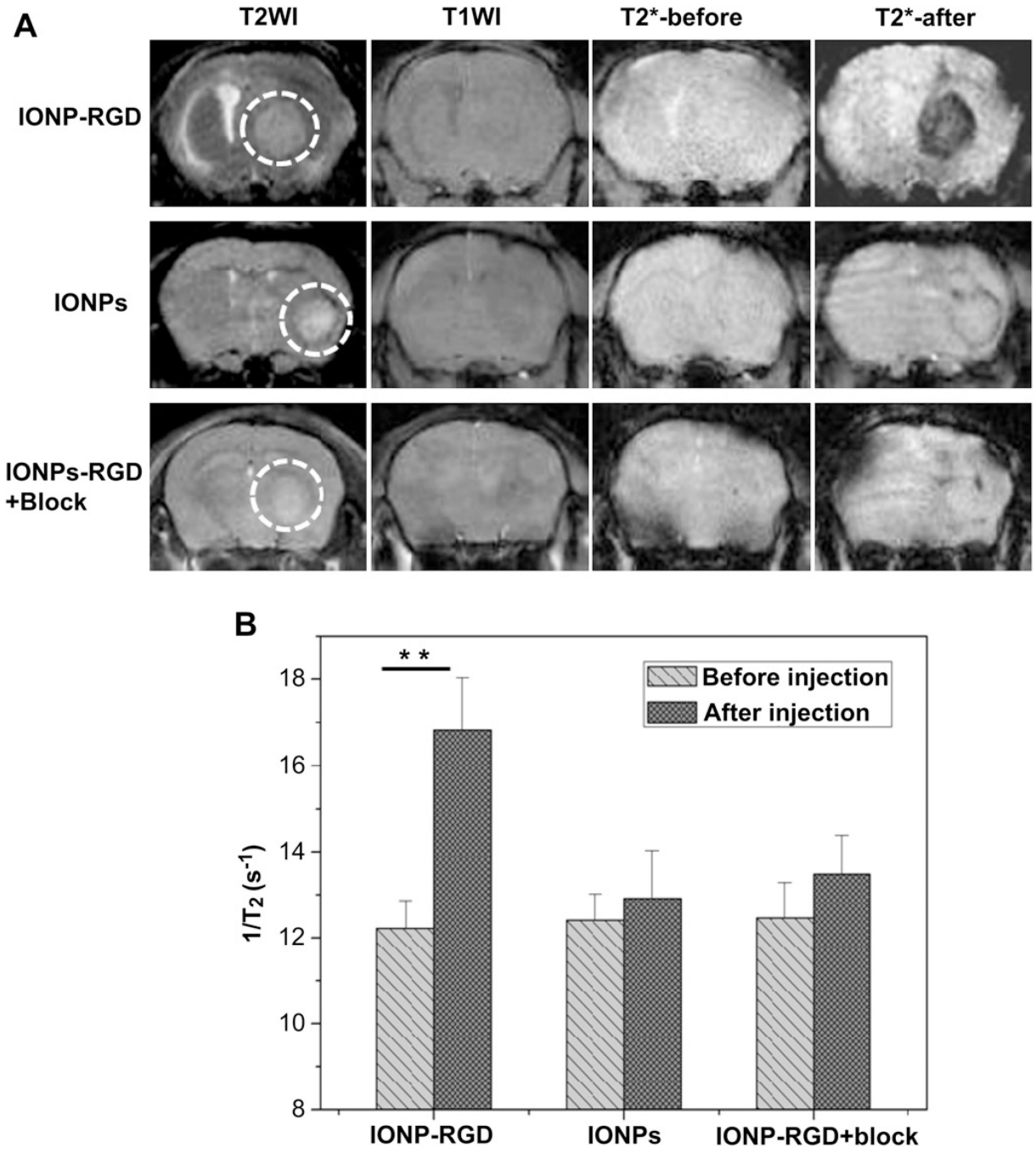

Fig. 4.

T_2^*-weighted MR images of nude mice bearing orthotopic U87MG glioblastoma (A) T_2^*-weighted MR images were acquired before and after injection of IONPs, IONP-RGD and IONP-RGD + block, respectively (B) Quantitative analysis of T_2^*-weighted MR images in tumor areas.

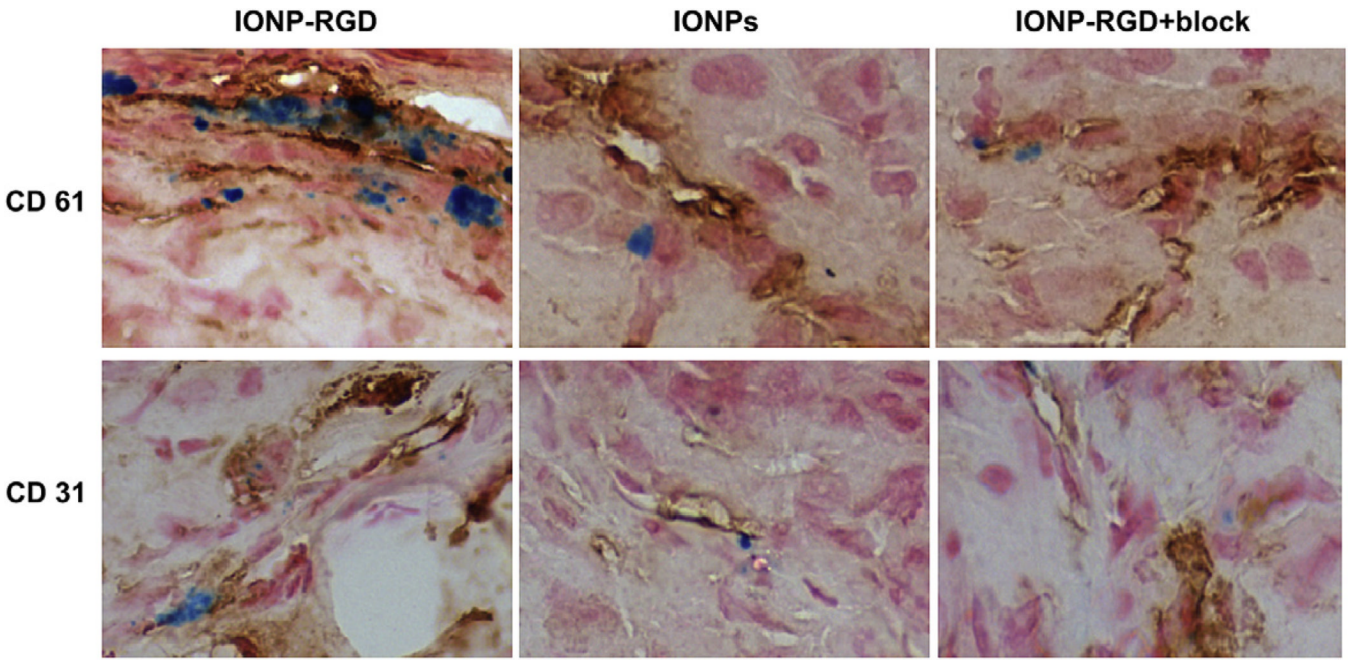

Fig. 5.

Prussian blue and CD31/CD61 double staining of the tumor sections. At 6 h post-injection, the mice were sacrificed and frozen tissue slices were prepared.

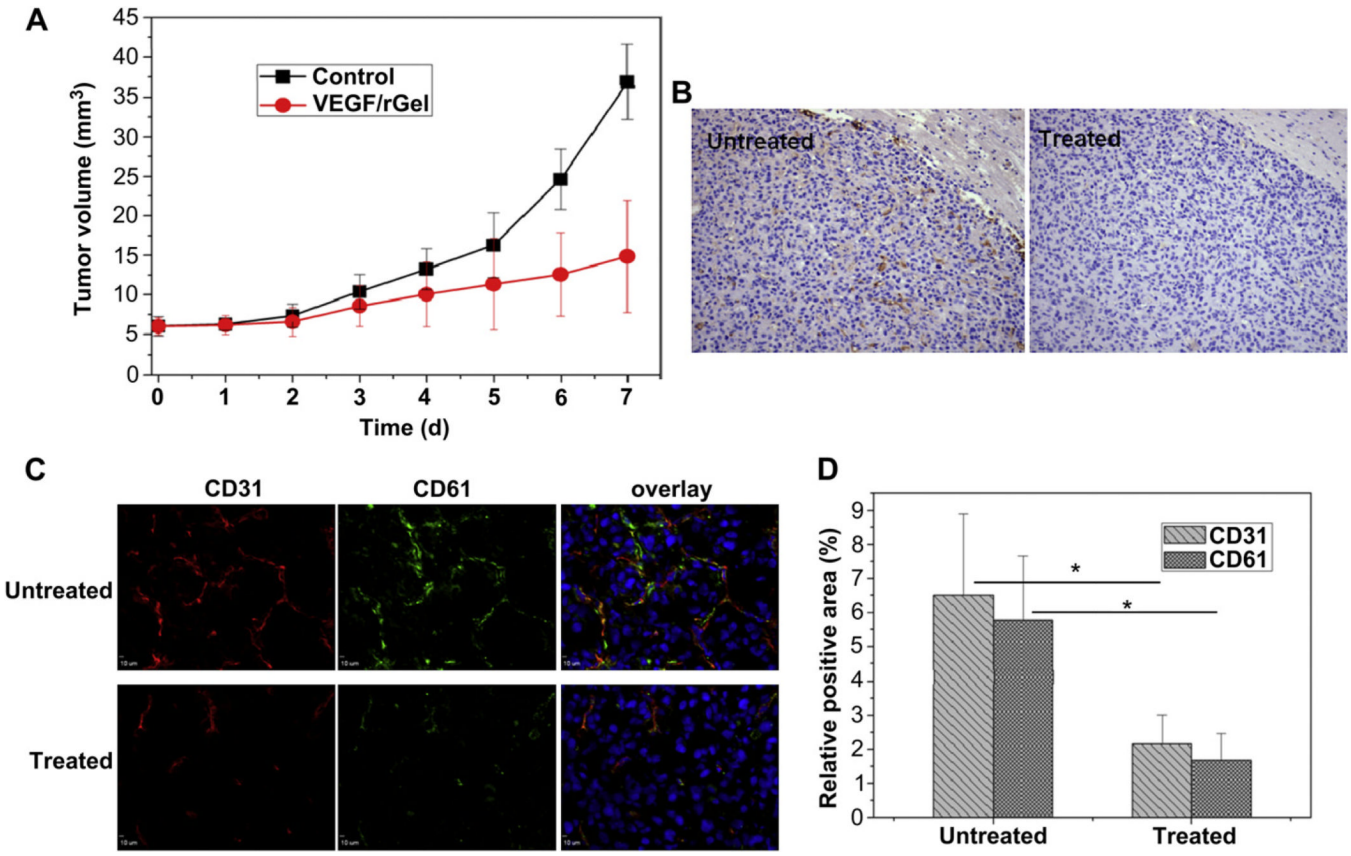

Fig. 6.

The effect of $VEGF_{121}$/rGel on the integrin $\alpha_v\beta_3$ expression of tumor angiogenic blood vessels (A) Tumor growth curves of untreated and $VEGF_{121}$/rGel treated groups were analyzed by MRI (B) CD31 staining of tumor angiogenic blood vessels by immnohistochemistry (C) CD31/CD61 double staining of tumor angiogenic blood vessels and integrin $\alpha_v\beta_3$ expression on frozen tissue slices (D) Quantitative analysis of CD31- and CD 61-positive area using Image J software (5 mice each group).

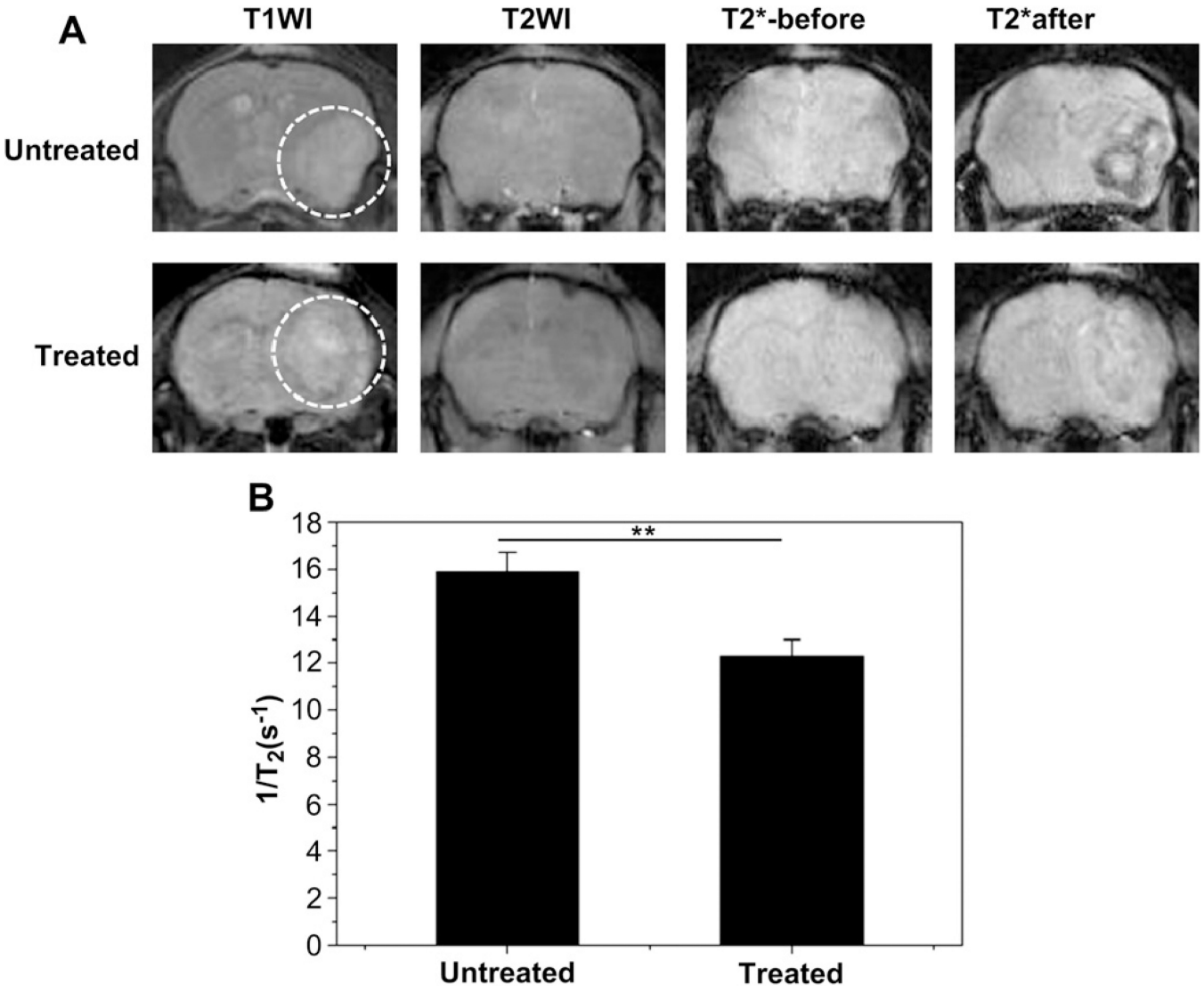

Fig. 7.

Monitoring of therapeutic response of $VEGF_{121}$/rGel using IONP-RGD in orthotopic U87MG glioblastoma model (A) T_2^*-weighted MR images of untreated and $VEGF_{121}$/rGel treated groups were acquired before and after injection of IONP-RGD (B) Quantification analysis of T_2^*-weighted MR images. The white circle indicates location of the implanted tumor (4 mice each group).

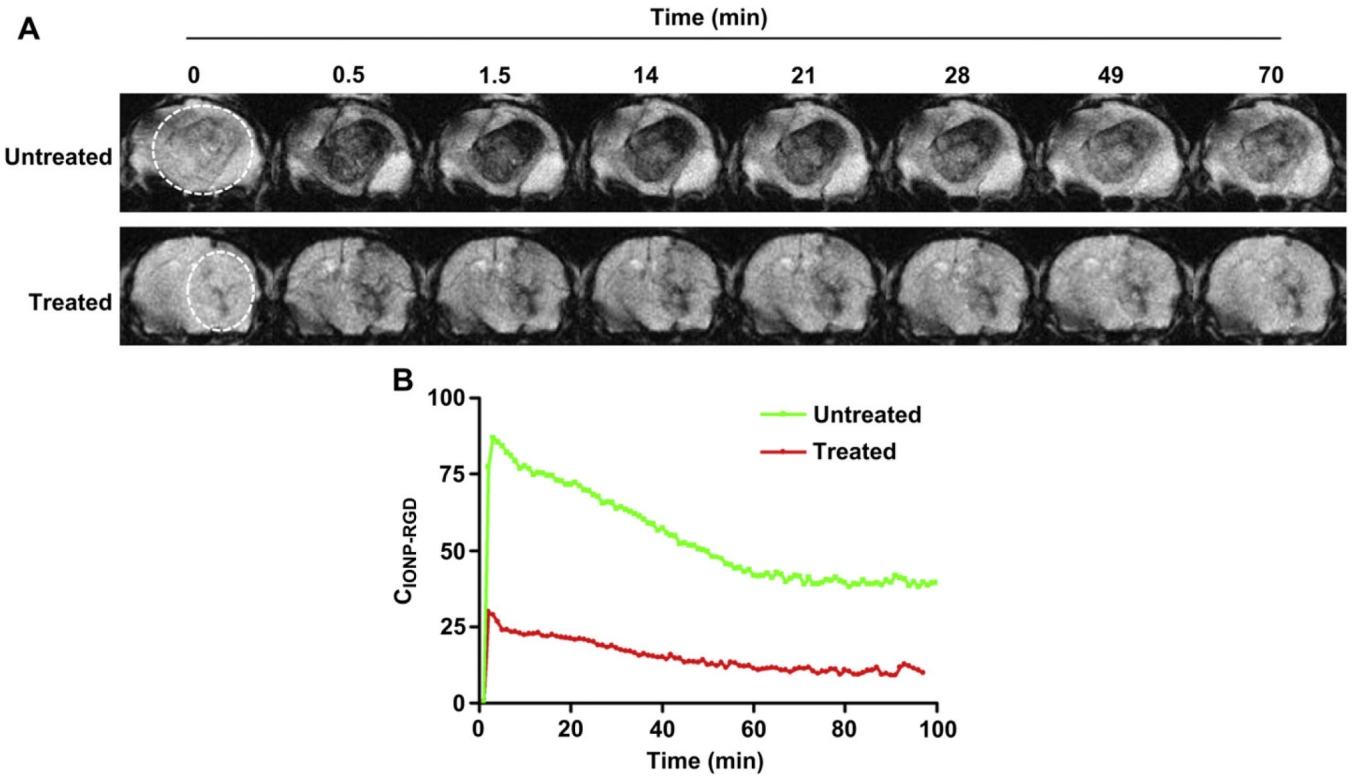

Fig. 8.

Dynamic monitoring of therapeutic response of $VEGF_{121}$/rGel using IONP-RGD in orthotopic U87MG glioblastoma model (A) T_2^*-weighted MR dynamic images of untreated and $VEGF_{121}$/rGel treated groups were acquired before and after injection of IONP-RGD (B) Quantitative analysis of T_2^*-weighted MR dynamic images (4 mice each group).